ACS APPLIED MATERIALS & INTERFACES

Research Article

www.acsami.org

Carbon-Nanotube-Encapsulated FeF_2 Nanorods for High-Performance Lithium-Ion Cathode Materials

Jisheng Zhou,[†,‡] Di Zhang,[†] Xiaoting Zhang,[†] Huaihe Song,*[,†] and Xiaohong Chen[†]

[†]State Key Laboratory of Chemical Resource Engineering, Key Laboratory of Carbon Fiber and Functional Polymers, Ministry of Education, Beijing University of Chemical Technology, Beijing, People's Republic of China

[‡]Changzhou Institute of Advanced Materials, Beijing University of Chemical Technology, Jiangsu, People's Republic of China

Supporting Information

ABSTRACT: Application of iron fluoride, a promising candidate of cathode materials for lithium ion batteries, is being hindered by its poor electrochemical performance caused by low electronic conductivity and large volume change. Design of carbon-encapsulated transitional metal compounds (including fluoride, oxide, sulfide, etc.) structure is one of the most effective strategies in improving their lithium-ion storage performance. In this work, we successfully synthesize for the first time carbon-nanotube-encapsulated FeF_2 nanorods via a facile in situ co-pyrolysis of ferrocene and NH_4F. This kind of core/shell carbon nanotube/FeF_2 nanorod exhibits better cyclic stability and rate-performance used as cathode materials. Better electrochemical performance of the nanorods should be attributed to the protection of the carbon shell because, experimentally, it is observed that outer carbon shells suffer from high internal stress during Li-ion insertion but efficiently keep the nanorods in the one-dimensional morphology and make nanorods a good electrical contact with the conductive carbon black. This work not only prepares high-performance core/shell carbon/iron fluoride cathode materials, but should also open a facile pathway for design of various novel nanostructures of other metal fluoride/carbon core/shell structures for future lithium-ion batteries.

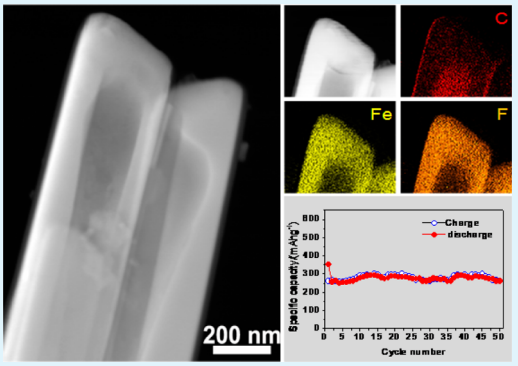

KEYWORDS: *iron fluoride, carbon nanotube, cathode, lithium-ion batteries, encapsulation, co-pyrolysis*

1. INTRODUCTION

Iron fluoride is one of the most potential candidates used as cathode materials due to its high specific capacity, low cost, and low toxicity.[1−6] Theoretical capacities of FeF_3 and FeF_2 are ca. 712 and 571 mA h g^{-1}, and their thermodynamic reduction potential with Li are ca. 2.74 and 2.66 V, respectively.[1−6] Many iron fluoride nanocomposites or nanostructures have been developed.[1−6] However, iron fluoride has the inherent defect of low electronic conductivity due to the high ionic state of Fe−F bonds. To improve the electrochemical activity, most efforts have been devoted to preparing carbon/iron fluoride composites by high-energy ball-milling of iron fluoride and traditional carbon materials such as carbon black, active carbon, or graphite.[1−3] With the development of nanocarbons, composites of iron fluoride and novel nanocarbons such as carbon nanotubes,[7] ordered mesoporous carbons,[8] and graphene nanosheets[9,10] have also been prepared. At present, design of new carbon-based iron fluoride nanostructures is becoming an interest topic.

Iron fluoride in carbon-based iron fluoride nanocomposites obtained in previous reports will be directly exposed to the electrolyte, so it may be difficult to form stable phase interface between carbon and iron fluoride. Thus, volume change will lead to exfoliation of iron fluoride from carbon or the current collector and even to the structural collapse, ultimately resulting in capacity fading and poor cyclic performance.[11] Construction of carbon-encapsulated transitional metal fluoride (TMF@C) structure should be one of the most effective strategies in improving the electrochemical performance of fluoride,[12] which has been used successfully to resolve the problems of both low conductivity and pulverization of both anode[13−19] and cathode[20,21] materials of transitional metal oxide, as shown by our previous reports[13,14] and other references.[15−21] On one hand, carbon shell with moderate electronic conductivity can ensure good electronic transport during the cycling process.[13−21] On the other hand, a confined space of carbon shell can not only efficiently buffer the volume change but can also be helpful in forming a stable contact between active materials and the inner surface of the carbon shell.[13−21] However, compared with facile preparation of carbon-encapsulated transitional metal oxide nanostuctures by simple pyrolysis of organic carbon sources, it is a big challenge to synthesize TMF@C because metal fluoride will decompose in the higher temperature, as described by Reddy et al.[11] Reddy and co-workers have also prepared carbon−FeF_2 nanocomposites with a more stable interface using CFx as inorganic carbon

Received: September 11, 2014
Accepted: November 17, 2014
Published: November 17, 2014

resources,[11] but no FeF_2@C core/shell nanostructures were obtained. Prakash et al.[12] also synthesized a complex carbon/Fe/Fe_3C/LiF nanocomposite by pyrolysis of a mixture of ferrocene and LiF in which the carbon matrix is consisted of multiwalled carbon nanotubes and carbon nano-onions; Fe and Fe_3C nanoparticles are encapsulated in the carbon matrix, while LiF is only simply dispersed within the carbon matrix rather than is encapsulated by carbon. Qiu et al. has prepared carbon-nanotube-encapsulated CeF_3 nanowires by an arc-discharge method using graphite and CeF_3 as raw materials,[22] which is only one case for a fluoride of a rare-earth metal, but it is difficult to employ an arc-discharge method to synthesize TMF@C nanostructures due to its high temperature during the preparation process.[22] Preparation of TMF@C has been very limited until now, although it has take great efforts to prepare carbon/transition metal−fluoride composites.[1−3,7−12] Very recently, He and co-workers reported the successful preparation of FeF_2@C nanorods by a one-pot thermal reaction using a mixture of ferrocene and polyvinylidene fluoride as precursor.[23] However, although perfect carbon-enecapsulation layers on the FeF_2 were formed, the carbon shell was so thick that lithium ion diffusion into the composite was restricted.[23] In addition, FeF_2 cores were fully filled in the carbon shells, so there was not enough buffer space for volume expansion of FeF_2 during the lithiation reactions. These structural drawbacks mean that the capability of carbon-encapsulated core−shell structures in enhancing the electrochemical performance of FeF_2 is not fully activated. Therefore, it is still a challenge to design the TMF@C cathode materials with more favorable microstructures for lithium-ion diffusions.

Here, we report an in situ synthesis of carbon-nanotube-encapsulated FeF_2 nanorods (FeF_2@CNT) by co-pyrolysis of ferrocene and NH_4F at 500 °C for 3 h (see detailed Experimental Section), where the ferrocene is used as a carbon and iron source, while the NH_4F is used as a fluorine source. Compared with previous work by He and co-workers,[23] fluorine sources do not contain carbon elements, and carbon sources are only from ferrocene in this work, so carbon content in the C/FeF_2 composites is largely decreased. More important, as-prepared FeF_2@CNT nanorods have more interesting structures in which the outer CNT-coating layers have open end points and soft walls, and inner FeF_2 cores are not fully filled in the CNT space. Soft CNT walls and unfilled space are beneficial to buffer the volume change of FeF_2 during the lithiation/delithiation reactions, while open end points of outer CNT-coating layers provide more accessible entry for lithium ion diffusion into the composites. Therefore, as-prepared FeF_2@CNT nanorods not only exhibit a higher reversible specific capacity but also have better rate-performance compared with the electrochemical performance of FeF_2@C nanorods in the previous report.[23] The approach used here is a very facile and scalable one-step process that can yield large-mass FeF_2@CNT nanorods with high quality, so it is also expected to be extended to prepare carbon-encapsulated other transitional metal fluorides.

2. EXPERIMENTAL SECTION

2.1. Preparation of FeF_2 Nanorods@Carbon Nanotube. The FeF_2@CNT nanorods were prepared by an in situ co-pyrolysis method, which is an effective technology for preparation of nanocarbon materials. In our previous work, we employed the ferrocene and other compounds (heavy oil,[24−26] durene,[27,28] and sulfur[29]) as sources via in situ co-pyrolysis in the autoclave to synthesize various nanocarbons such as carbon-encapsulated Fe_3C/Fe nanocrystals,[24−27] carbon-encapsulated FeS microspheres,[29] and quadrangular carbon nanotubes.[28] Considering the decomposition temperature of ferrocene (over 400 °C) and the temperature duration of the autoclave, the in situ co-pyrolysis preparation of nanocarbons is generally carried out in the range of 400−800 °C. Here, we used ferrocene and NH_4F as sources to prepare the FeF_2@CNT nanorods via a procedure similar to those in previous reports. Typically, ferrocene (2.5 mmol) and NH_4F (10 mmol) were mixed by grinding in an agate mortar. Then, the mixture of ferrocene and NH_4F was put into a 30 mL autoclave. After the air in the autoclave was replaced three times by pure Ar, the autoclave was sealed, and then the co-pyrolysis was carried out by heating the autoclave to 500 °C at a rate of 5 °C/min and maintaining the temperature at 500 °C for 3 h. After the reaction system cooled to room temperature, the obtained reaction products were washed with deionized water and then with acetone to remove the unreacted NH_4F and small molecular species. The obtained products were FeF_2@CNT. Further, carbon nanotubes were obtained after removing FeF_2 cores in FeF_2@CNT by HCl solution. For investigating the formation process of FeF_2@CNT, the other products were also prepared by annealing the mixtures of ferrocene and NH_4F at 450 °C for 3 h and at 700 °C for 10 and 40 min, respectively.

2.2. Characterization. The measurements on the bright-field transmission electron microscope (TEM), high-angle annular dark-field scanning transmission electron microscopy (HAADF-TEM) images, and corresponding high-resolution transmission electron microscope (HRTEM) images were carried out using Tecnai G2 F20 U-TWIN electron microscope with an accelerating voltage of 200 kV. Elemental dispersive spectroscopy (EDS) mappings were collected from an attached EDAX SDD EDS detector on the electron microscope (Tecnai G2 F20 U-TWIN) to determine the elemental distribution of C, F, and Fe in the nanorods under 200 kV. The F Kα peak often can be overlapped by the Fe Lα peak in EDS analysis. Overlapping elemental peaks were separated by peak deconvolution algorithms with an automatic routine in the EDS analysis sofware. The samples for TEM and HREM observations were prepared by dispersing the products in ethanol with an ultrasonic bath for 15 min, and then a few drops of the resulting suspension were placed on a nickel grid.

Scanning electron microscope (SEM) observation was conducted on a Hitachi S-4700 field emission scanning electron microscope.

X-ray diffraction (XRD) measurements were performed with a Rigaku D/max-2500B2+/PCX system using Cu Kα radiation (λ = 1.5406 Å) over the range of 5−90° (2θ) at room temperature.

2.3. Electrochemical Measurements. The electrochemical experiments were conducted in a CR2032 type cell, composed of a lithium sheet and a working electrode. The lithium sheet was used as both reference and counter electrodes. One molar $LiPF_6$ solution in a 1:1 (volume) mixture of ethylene carbonate (EC) and dimethyl carbonate (DMC) from Guotai Huarong Chemical New Material Co., Ltd., Jiangsu, China, was used as electrolyte. Working electrode was prepared by the following process: First, a slurry was prepared by mixing active mass (FeF_2@CNT, 80 wt %), carbonaceous additive (acetylene black, 10 wt %) and poly(vinylidene difluoride) (PVDF, 10 wt %). Then, the slurry was coated on the stainless steel plate. At last, working electrode was obtained by drying the stainless steel plate coated by slurry in a vacuum oven at 120 °C overnight and subsequently pressing the plate under ca. 10 MPa. Morphology of FeF_2@CNT in the working electrode after pressing is observed by SEM.

The cells were galvanostatically discharged (Li insertion) and charged (Li extraction) in the voltage range from 1.0 to 4.2 V versus Li/Li^+ at various current densities from 50 to 1000 Ag^{-1}. To observe the morphology change of FeF_2@CNT undergoing the discharge/charge, the cell is open, and working electrode after cycling is also investigated by SEM.

3. RESULTS AND DISCUSSION

3.1. Morphology and Structure of FeF_2@CNT Nanorods. Figure 1a exhibits the typical SEM image of the as-prepared FeF_2@CNT nanorods. The FeF_2@CNT nanorods own rod-like nanostructure with a length in the range of 2−4 μm and a diameter of 200−500 nm. The XRD pattern of FeF_2@CNT nanorods (Figure 2a) shows that all of peaks belong to FeF_2, indicating the high phase-purity of FeF_2 obtained. It can be seen from SEM images (Figure 1a and Figure S1, Supporting Information) that the nanorods have an almost transparent shell under the electron beam. TEM image (Figure 1b) also confirms the core/shell structure of the FeF_2@CNT. Furthermore, HRTEM images reveal that the shell is composed of turbulent carbon layers (Figure 1c), and the inner core region has a multicrystal structure (Figure 1d) in which the lattice of 3.4 and 2.6 Å correspond to (110) and (101) lattice spacing of FeF_2, respectively. Besides, the observed end point of the FeF_2 nanorod is not fully coated by carbon shell.

HAADF-STEM images and elemental mapping (Figure 1e) reveal the clearer inner structure and detailed elemental distribution of the FeF_2@CNT. Interestingly, HAADF-STEM image of the nanowire shows the unfilled space of the inner core, which corresponds to the low-contrast region in TEM image (Figure 1b). It needs to be stressed that nanorods with unfilled space can be seen frequently (Figure S2, Supporting Information), which can be helpful to buffer the volume change of FeF_2 during Li storage.[13,14] EDS measurement reveals that FeF_2@CNT is composed of C, Fe, and F elements (Figure S3, Supporting Information). Elemental mapping images (Figure 1 e,iii−v) clearly demonstrate that carbon is detected weakly at the core and in unfilled regions but strongly at the edge region, and Fe and F elements are detected strongly in the core region and away from shell and unfilled regions, indicating further that there is no FeF_2 in the unfilled region. These results indicate that the core consisting of Fe/F compound is coated by a carbon shell, which is in good agreement with bright-field observation.

To analyze in detail the structure of shell, we removed the FeF_2 cores using HCl. The XRD pattern of the residual carbon materials (Figure 2b) shows one peak at 26°, which should be attributed to turbulent graphene layers of the carbon shells. SEM images (Figure 3a,b) show that tube-like nanostructure of

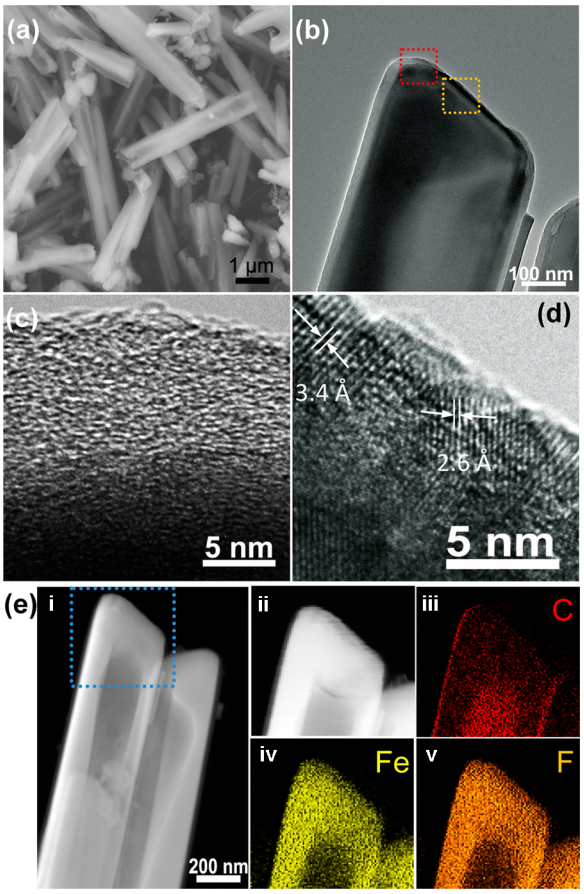

Figure 1. (a) SEM image of FeF_2@CNT obtained at 500 °C for 3 h, (b) bright-field TEM images of a typical FeF_2@CNT nanorod, (c) HRTEM images of shell area in red box of image b, (d) HRTEM image of core area in yellow box of image c, and (e, i) HAADF-STEM image of the nanowire shown in image b, (ii) HAADF-STEM image in blue box of image i and corresponding elemental mapping of (iii) C, (iv) Fe, and (v) F.

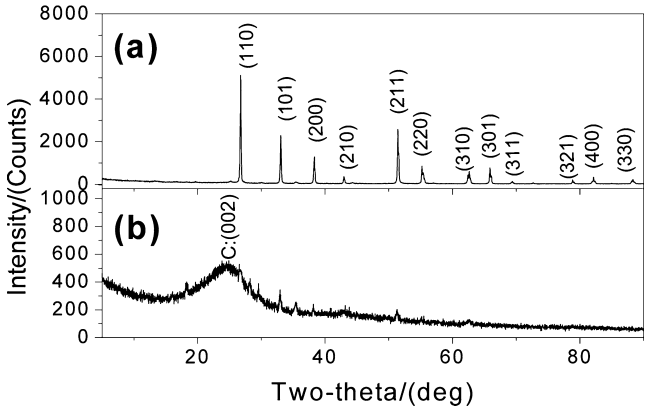

Figure 2. XRD pattern of (a) FeF_2@CNT obtained at 500 °C for 3 h and (b) CNTs obtained after removing FeF_2.

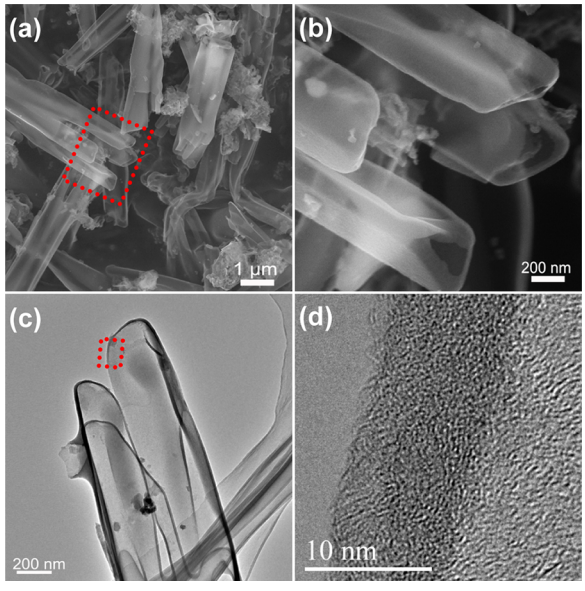

Figure 3. (a) SEM image of CNT obtained by removing the FeF_2 in FeF_2@CNT nanorods, (b) SEM image in the selected area in image a, (c) TEM image of CNT, and (d) HRTEM image of the wall of CNT in the selected area of image c.

dx.doi.org/10.1021/am506236n | ACS Appl. Mater. Interfaces 2014, 6, 21223−21229

carbon shell is well retained after the removal of FeF_2. Interestingly, it can be seen that the CNT shell can collapse when losing the support of interior FeF_2 rod, indicating that CNTs own soft walls, which can provide an effective buffer for volume changes caused by lithiation/delithiation when the FeF_2@CNT nanorods are used as electrode materials. Moreover, agreeing with the TEM observation of FeF_2@CNT (Figure 1b,d), the end point of the obtained CNT is open. Compared with the closed end point of FeF_2@C obtained by annealing ferrocene and PVDF,[23] the open end point of FeF_2@CNT can be more beneficial to the inward/outward diffusion of Li ion in the iron fluoride.[28] In addition, the TEM image shows that the average thickness of the shell is ca. 10 nm (Figure 3c), which is also thinner than that of carbon shells described in ref 23. The HRTEM image (Figure 3d) show that the wall of the nanotube is a semigraphitic structure, which is consistent with the above analysis (Figure 1b,e). FeF_2 content in the FeF_2@CNT nanorods were calculated to be ca. 71 wt % by TG measurement (Figure S4, Supporting Information).

3.2. Formation Mechanism of FeF_2@CNT Nanorods. It is very interesting to consider how the FeF_2@CNT grows up because this process involves not only the growth of iron fluoride cores but also the formation of carbon shells coating the cores. At 450 °C for 3 h, only short nanorods and nanoparticles are found (Figure S5, Supporting Information). The carbon shell on the particles is very thin or even lacking on some particles. Therefore, the formation mechanism of FeF_2@CNT can be described by Figure 4. First, ferrocene will be decomposed into clusters of iron and carbon atoms and hydrocarbons[24−28,30−32] (Figure 4b). Then, iron clusters will react with NH_4F into short FeF_2 nanorods (Figure 4c). FeF_2 may play the role of catalyst in the growth of carbon shells (Figure 4d). Also, the catalytic ability of FeF_2 is related to temperature. At low temperature (450 °C), catalytic activity of FeF_2 is very low, and partial, bare, short nanorods are found. At suitable temperature, the turbulent carbon shells will preferentially form on the surface of FeF_2, as shown in Figures 2 and 3. Even at 700 °C for 10 min, FeF_2@CNT nanorods are also obtained, and very interestingly, the nanostructures of CNT-coated many FeF_2 nanoparticles can be found easily due to the shorter growth time (Figure 5 and Figure S6, Supporting Information). Therefore, it can be deduced that the carbon shells are grown first and then FeF_2 nanoparticles are filled into the hollow inner of carbon shells, as shown in Figure 4e, and carbon shells play a crucial role of template in the subsequent growth of one-dimensional FeF_2 nanorods. Compared with the closed end point and thicker shells formed in the reaction system of ferrocene and PVDF, open end point and thinner shells of FeF_2@CNT are facile to be obtained in the system of ferrocene and NH_4F due to less carbon sources. However, at 700 °C and when time is prolonged to 40 min, FeF_2 is decomposed fully into α-Fe and even becomes Fe_3C by reacting with C (Figure S7, Supporting Information). These results indicate that the appropriate reaction temperature for FeF_2@CNT nanorods should be limited in the range of 450−700 °C. Here, we emphasize that the formation mechanism in the case of FeF_2@CNT is obviously different from the well-known dissolution/precipitation mechanism of metal@C nanostructures.[24−27,31,32] Additionally, carbon-coated other metal fluoride structures may also be prepared by a similar in situ approach.

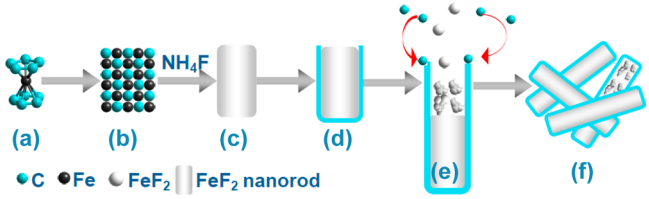

Figure 4. Schematic illustration of formation process of FeF_2@CNT nanorods.

3.3. Electrochemical Performance of FeF_2@CNT Nanorods. The electrochemical performance of FeF_2@CNT was evaluated by galvanostatic charge/discharge measurements. Figure 6a shows the initial two charge/discharge curves of FeF_2@CNT electrode, which are very similar to the previous reports.[4,11,23,33] There are two lithiation regions in the initial discharge curve. The first region is a slope from open circuit voltage to ca. 1.6 V, which should be attributed to insertion of Li ion into the Fe^{3+} impurities to form $Li_{2x}Fe_{1-x}F_2$.[4,33] The Fe^{3+} impurities may be attributed to the exposure of FeF_2@CNT nanorods to air. However, no obvious impurity phase is observed in the XRD pattern (Figure 2a) due to the protection of outer carbon shells, so the discharged specific capacity in the first region is only ca. 25 mA h g^{-1}, indicating no obvious Li-

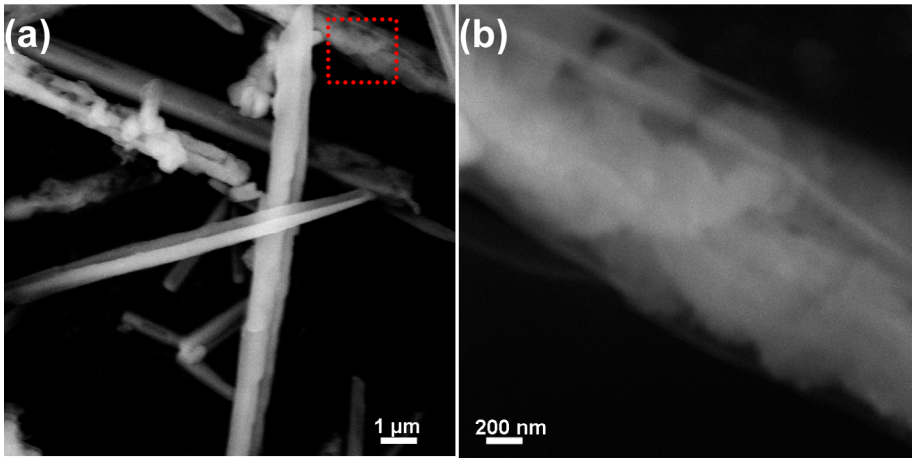

Figure 5. (a) SEM image of the sample obtained by co-pyrolysis of ferrocene and NH_4F at 700 °C for 10 min, and (b) magnified SEM image of red box in the image a, which shows that many aggregated FeF_2 nanoparticles are coated in the thin CNT shell.

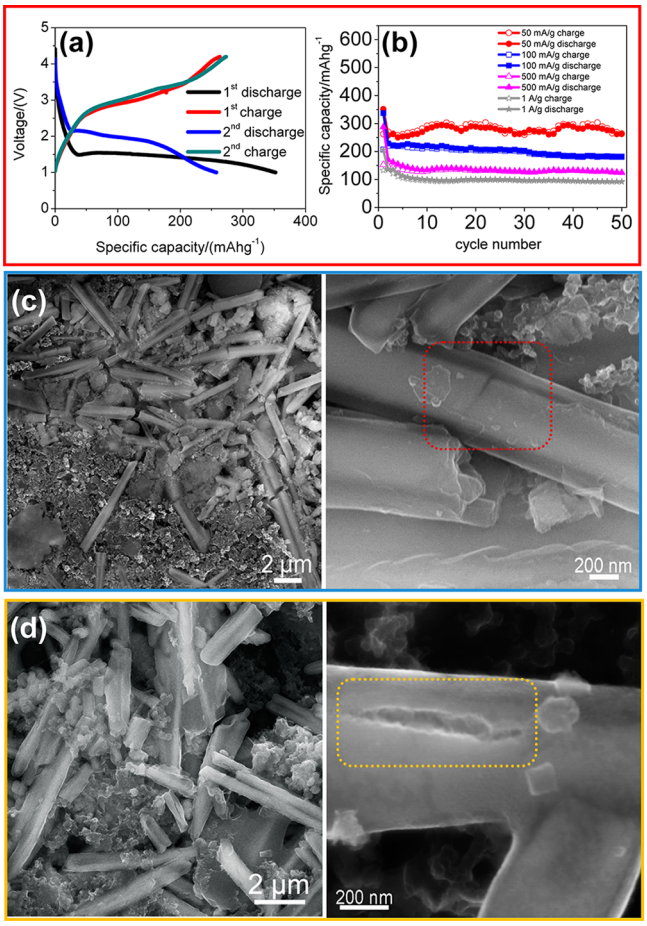

Figure 6. (a) The initial two charge/discharge curves and (b) cycling performance of FeF_2@CNT at various current densities, and SEM images of FeF_2@CNT electrode plate (c) before and (d) after charge/discharge of 50 cycles at the current density of 50 mA g^{-1}.

intercalation reaction, which is also consistent with previous reports.[4,33] The second lithiation region in the first discharge curve is a redox plateau at ca. 1.6 V, which should be attributed to the conversion reaction from FeF_2 to α-Fe.[4,11,23,33] However, in the second discharge curve, the voltage plateau increases to ca. 2.2 V, which is ascribed to the reduction of particle size after the first lithiation of FeF_2.[4] The charge voltage plateau keeps in the range of 2.5 to 4.0 V for the first and second charge processes, corresponding to the reconversion from α-Fe to FeF_2.[4,33] The first discharge capacity is ca. 352 mA h g^{-1} at 50 m A g^{-1}, which is ca. 87% of theoretical capacity (405 mA h g^{-1}) of FeF_2@CNT calculated via 571 mA h g^{-1} of FeF_2 multiplied by its content of 71 wt % in the composite.

FeF_2@CNT electrode exhibits better cycle stability and high-rate performance. At 50 mA g^{-1}, the first reversible capacity (C_{rev}) of FeF_2@CNT is ca. 263 mA h g^{-1}. After 50 cycles, there is almost no capacity fading. At 100 mA g^{-1}, the first C_{rev} is ca. 221 mA h g^{-1} (Figure 6b), which is 84% of that at 50 mA g^{-1}, and the C_{rev} remains 181 mA h g^{-1} after 50 cycles. It can be found that at the smaller current densities, the specific capacities of our FeF_2@CNT nanorods is similar to that of the FeF_2@C nanorods in He and co-workers' work (Table S1, Supporting Information),[23] where the first reversible capacities at 50 and 100 mA g^{-1} were 314 and ca. 200 mA h g^{-1}, respectively. However, the capacity of FeF_2@C nanorods at 50 mA g^{-1} was decreased into 217 mA h g^{-1}, indicating that our FeF_2@CNT nanorods own better cycling stability. In addition, the cycling performance of core/shell FeF_2/C nanocomposites shown both in our work and in He and co-workers' work[23] is better than that of bare iron fluoride and iron fluoride/C composites without a core/shell structure (Table S1, Supporting Information). For example, in previous reports, the FeF_3 nanowires[34] or FeF_2/CFx composites[11] exhibit higher initial C_{rev}, but they suffer from fast capacity fading. For example, C_{rev} of reported FeF_2/CFx composites can reach 422 mA h g^{-1} at the first cycle but fade quickly to 171 mA h g^{-1} after 25 cycles at 22.7 mA g^{-1} in the voltage window of 1.3−4.3 V at 25 °C.[11] FeF_3 nanowires without carbon coating yield a capacity as high as 543 mA h g^{-1} at the first cycle and retain a capacity of 223 mA h g^{-1} after 50 cycles at 50 mA g^{-1} at room temperature.[34]

Moreover, at the higher current densities, the electrochemical performance of our FeF_2@CNT nanorods is much better than that of the FeF_2@C nanorods in He and co-workers' work.[23] At 500 mA g^{-1} and 1 Ag^{1-}, the first reversible capacities of FeF_2@CNT nanorods are still up to 153 mA h g^{-1} and 133 mA h g^{-1}, respectively. However, the reversible capacities of FeF_2@C nanorods[23] at 500 mA g^{-1} and 1 Ag^{1-} were ca. 100 and 50 mA h g^{-1}, respectively, which are obviously lower than those of FeF_2@CNT nanorods. After 50 cycles, the reversible capacities of FeF_2@CNT nanorods at 500 mA g^{-1} and 1 Ag^{1-} remain at 124 and 92 mA h g^{-1}, which are 81 and 69% of the corresponding first C_{rev}, respectively, indicating better cyclic stability at high-rate. In addition, the rate-performance of FeF_2@CNT nanorods here is even comparable with those of graphene/CNT-based FeF_3 cathode materials (Table S1, Supporting Information).[7,9,10]

Based on the analysis of electrochemical performance, better cyclic stability and rate-performance of FeF_2@CNT nanorods should be attributed to the protection of CNT shells and their special microstructures, including unfilled inner-space and open end points. On one hand, open end points and thinner walls of the CNT shells, as well as unfilled space of FeF_2@CNT nanorods in this work, can favor the diffusion of Li ions, while thick carbon shells and complete coating of FeF_2@C will block the diffusion of Li ions into the composite.[23] Therefore, here, FeF_2@CNT nanorods exhibit much a better rate performance than that of FeF_2@C nanorods.[23] On the other hand, FeF_2@CNT nanorods retain their stable structures, which is beneficial to the improvement of cyclic stability during the discharge/charge processes. Before cycling, SEM image of FeF_2@CNT are laid on the plate (Figure 6c). And some inner FeF_2 nanorods have been snapped off under the pressure of 10 MPa (see the Experimental Section), but outer carbon shells remain intact due to their flexible structure, as shown in the red box of Figure 4c. After 50 cycles, the FeF_2@CNT remains the morphology of one-dimensional nanorods (Figure 6d), and a clearer SEM image (yellow box of Figure 6d) shows that a crack appears on the carbon shell, implying the high internal stress during Li-ion insertion. However, the nanorods still keep good electrical contact with the conductive carbon black, indicating that outer flexible carbon shells and unfilled inner-space can efficiently buffer phase transformation of FeF_2 and prevent the active materials from falling off the electrode.

4. CONCLUSION

In summary, FeF_2@CNT nanorods have been synthesized successfully via a facile in situ co-pyrolysis of ferrocene and NH_4F. When they are used as cathode materials for LIBs,

FeF_2@CNT nanorods exhibit a higher specific capacity, better cyclic stability and better high-rate performance, which should be attributed to the protection of the CNT shell and special microstructures of FeF_2@CNT nanorods, including unfilled inner-space and open end point. These novel core−shell structures are also expected to be applied in supercapacitors and catalysts, for example.

■ ASSOCIATED CONTENT

Supporting Information

TG curve, XRD patterns, and TEM and SEM images of FeF_2@CNT nanorods obtained at various conditions. This material is available free of charge via the Internet at http://pubs.acs.org.

■ AUTHOR INFORMATION

Corresponding Author

*E-mail: songhh@mail.buct.edu.cn.

Notes

The authors declare no competing financial interest.

■ ACKNOWLEDGMENTS

This work was supported by the Natural Science Foundation of Jisangsu Province of China (BK20140269), the National Natural Science Foundation of China (51202009 and 51272019), the New Teachers' Fund for Doctor Stations, Ministry of Education of China (20120010120004), and the Foundation of Excellent Doctoral Dissertation of Beijing City (YB20121001001).

■ REFERENCES

(1) Badway, F.; Pereira, N.; Cosandey, F.; Amatucci, G. G. Carbon-Metal Fluoride Nanocomposites Structure and Electrochemistry of FeF_3:C. *J. Electrochem. Soc.* **2003**, *150*, A1209−A1218.

(2) Badway, F.; Cosandy, F.; Pereira, N.; Amatucci, G. G. Carbon Metal Fluoride Nanocomposites High-Capacity Reversible Metal Fluoride Conversion Materials as Rechargeable Positive Electrodes for Li Batteries. *J. Electrochem. Soc.* **2003**, *150*, A1318−A1327.

(3) Plitz, I.; Badway, F.; Al-Sharab, J.; DuPasquier, A.; Cosandey, F.; Amatucci, G. G. Structure and Electrochemistry of Carbon-Metal Fluoride Nanocomposites Fabricated by Solid-State Redox Conversion Reaction. *J. Electrochem. Soc.* **2005**, *152*, A307−A315.

(4) Wang, F.; Robert, R.; Chernova, N. A.; Pereira, N.; Omenya, F.; Badway, F.; Hua, X.; Ruotolo, M.; Zhang, R.; Wu, L.; Volkov, V.; Su, D.; Key, B.; Whittingham, M. S.; Grey, C. P.; Amatucci, G. G.; Zhu, Y.; Graetz, J. Conversion Reaction Mechanisms in Lithium Ion Batteries: Study of the Binary Metal Fluoride Electrodes. *J. Am. Chem. Soc.* **2011**, *133*, 18828−18836.

(5) Li, C.; Gu, L.; Tsukimoto, S.; Tsukimoto, S.; Aken, P. A.; Maier, J. Low-Temperature Ionic-Liquid-Based Synthesis of Nanostructured Iron-Based Fluoride Cathodes for Lithium Batteries. *Adv. Mater.* **2010**, *22*, 3650−3654.

(6) Li, C.; Gu, L.; Tong, J.; Tsukimoto, S.; Maier, J. A Mesoporous Iron-Based Fluoride Cathode of Tunnel Structure for Rechargeable Lithium Batteries. *Adv. Funct. Mater.* **2011**, *21*, 1391−1397.

(7) Kim, S.-W.; Seo, D.-H.; Gwon, H.; Kim, J.; Kang, K. Fabrication of FeF_3 Nanoflowers on CNT Branches and Their Application to High Power Lithium Rechargeable Batteries. *Adv. Mater.* **2010**, *22*, 5260−5264.

(8) Jung, H.; Shin, J.; Chae, C.; Lee, J. K.; Kim, J. FeF_3/Ordered Mesoporous Carbon (OMC) Nanocomposites for Lithium Ion Batteries with Enhanced Electrochemical Performance. *J. Phys. Chem. C* **2013**, *117*, 14939−14946.

(9) Zhao, X.; Hayner, C. M.; Kung, J. C.; Kung, H. H. Photothermal-Assisted Fabrication of Iron Fluoride-Graphene Composite Paper Cathodes for High-Energy Lithium-Ion Batteries. *Chem. Commun.* **2012**, *48*, 9909−9911.

(10) Chu, Q.; Xing, Z.; Ren, X.; Asiri, A. M.; Al-Youbi, A. O.; Alamry, K. A.; Sun, X. Reduced Graphene Oxide Decorated with FeF_3 Nanoparticles: Facile Synthesis and Application as a High Capacity Cathode Material for Rechargeable Lithium Batteries. *Electrochim. Acta* **2013**, *111*, 80−85.

(11) Reddy, M. A.; Breitung, B.; Chakravadhanula, V. S. K.; Wall, C.; Engel, M.; Kübel, C.; Powell, A. K.; Hahn, H.; Fichtner, M. CF_x Derived Carbon-FeF_2 Nanocomposites for Reversible Lithium Storage. *Adv. Energy Mater.* **2013**, *3*, 308−313.

(12) Prakash, R.; Mishra, A. K.; Roth, A.; Kübel, C.; Scherer, T.; Ghafari, M.; Hahn, H.; Fichtner, M. A Ferrocene-Based Carbon-Iron Lithium Fluoride Nanocomposite as a Stable Electrode Material in Lithium Batteries. *J. Mater. Chem.* **2010**, *20*, 1871−1876.

(13) Zhou, J.; Song, H.; Chen, X.; Zhi, L.; Yang, S.; Huo, J.; Yang, W. Carbon-Encapsulated Metal Oxide Hollow Nanoparticles and Metal Oxide Hollow Nanoparticles: A General Synthesis Strategy and Its Application to Lithium-Ion Batteries. *Chem. Mater.* **2009**, *21*, 2935−2940.

(14) Zhou, J.; Song, H.; Chen, X.; Huo, J. Diffusion of Metal in a Confined Nanospace of Carbon Nanotubes Induced by Air Oxidation. *J. Am. Chem. Soc.* **2010**, *132*, 11402.

(15) Zhang, W.; Wu, X.; Hu, J.; Guo, Y.; Wan, L. Carbon Coated Fe_3O_4 Nanospindles as a Superior Anode Material for Lithium-Ion Batteries. *Adv. Funct. Mater.* **2008**, *18*, 3941−3946.

(16) Wu, P.; Du, N.; Zhang, H.; Yu, J.; Yang, D. Carbon Nanocapsules as Nanoreactors for Controllable Synthesis of Encapsulated Iron and Iron Oxide: Magnetic Properties and Reversible Lithium Storage. *J. Phys. Chem. C* **2011**, *115*, 3612−3620.

(17) Yu, W.-J.; Hou, P.-X.; Zhang, L.-L.; Li, F.; Liu, C.; Cheng, H.-M. Preparation and Electrochemical Property of Fe_2O_3 Nanoparticles-Filled Carbon Nanotubes. *Chem. Commun.* **2010**, *46*, 8576−8578.

(18) Zhang, L.; Wu, H. B.; Liu, B.; Lou, X. W. (David) Formation of Porous SnO_2 Microboxes via Selective Leaching for Highly Reversible Lithium Storage. *Energy Environ. Sci.* **2014**, *7*, 1013−1017.

(19) Gao, G.; Yu, L.; Wu, H. B.; Lou, X. W. (D.) Hierarchical Tubular Structures Constructed by Carbon-Coated α-Fe_2O_3 Nanorods for Highly Reversible Lithium Storage. *Small* **2014**, *10*, 1741−1745.

(20) Ni, J.; Gao, L.; Lu, L. Carbon Coated Lithium Cobalt Phosphate for Li-Ion Batteries: Comparison of Three Coating Techniques. *J. Power Sources* **2013**, *221*, 35−41.

(21) Wang, J.; Sun, X. Understanding and Recent Development of Carbon Coating on $LiFePO_4$ Cathode Materials for Lithium-Ion Batteries. *Energy Environ. Sci.* **2012**, *5*, 5163−5185.

(22) Wang, Z.; Zhao, Z.; Qiu, J. Carbon Nanotube Templated Synthesis of CeF_3 Nanowires. *Chem. Mater.* **2007**, *19*, 3364−3366.

(23) Zhang, J.; Wang, L.; Li, J.; Wen, L.; He, X. A One-Pot Approach Toward FeF_2−Carbon Core−Shell Composite and Its Application in Lithium Ion Batteries. *J. Alloys Compd.* **2014**, *606*, 226−230.

(24) Huo, J.; Song, H.; Chen, X. Preparation of Carbon-Encapsulated Iron Nanoparticles by Co-carbonization of Aromatic Heavy Oil and Ferrocene. *Carbon* **2004**, *42*, 3177−3182.

(25) Huo, J.; Song, H.; Chen, X.; Lian, W. Formation and Transformation of Carbon-Encapsulated Iron Carbide/Iron Nanorods. *Carbon* **2006**, *44*, 2849−2852.

(26) Wu, B.; Song, H.; Zhou, J.; Chen, X. Formation Mechanism of Carbon-Encapsulated Iron Nanorods in a Co-carbonization Process. *Carbon* **2011**, *49*, 890−894.

(27) Song, H.; Chen, X. Large-Scale Synthesis of Carbon-Encapsulated Iron Carbide Nanoparticles by Co-carbonization of Durene with Ferrocene. *Chem. Phys. Lett.* **2003**, *374*, 400−404.

(28) Zhou, J.; Song, H.; Fu, B.; Wu, B.; Chen, X. Synthesis and High-Rate Capability of Quadrangular Carbon Nanotubes with One Open End as Anode Materials for Lithium-Ion Batteries. *J. Mater. Chem.* **2010**, *20*, 2794−2800.

(29) Wu, B.; Song, H.; Zhou, J.; Chen, X. Iron Sulfide-Embedded Carbon Microsphere Anode Material with High-Rate Performance for Lithium-Ion Batteries. *Chem. Commun.* **2011**, *47*, 8653−8655.

(30) Zhang, J.; Du, J.; Qian, Y.; Yin, Q.; Zhang, D. Shape-Controlled Synthesis and Their Magnetic Properties of Hexapod-Like, Flake-Like, and Chain-Like Carbon-Encapsulated Fe_3O_4 Core/Shell Composites. *Mater. Sci. Eng., B* **2010**, *170*, 51−57.
(31) Wang, S.; Huang, X.; He, Y.; Huang, H.; Wu, Y.; Hou, L.; Liu, X.; Yang, T.; Zou, J.; Huang, B. Synthesis, Growth Mechanism, and Thermal Stability of Copper Nanoparticles Encapsulated by Multi-Layer Graphene. *Carbon* **2012**, *50*, 2119−2125.
(32) Lee, S.; Hong, J.; Koo, J. H.; Lee, H.; Lee, S.; Choi, T.; Jung, H.; Koo, B.; Park, J.; Kim, H.; Kim, Y.-W.; Lee, T. Synthesis of Few-Layered Graphene Nanoballs with Copper Cores Using Solid Carbon Source. *ACS Appl. Mater. Interfaces* **2013**, *5*, 2432−2437.
(33) Yamakawa, N.; Jiang, M.; Key, B.; Grey, C. P. Identifying the Local Structures Formed during Lithiation of the Conversion Material, Iron Fluoride, in a Li-Ion Battery: A Solid-State NMR, X-ray Diffraction, and Pair Distribution Function Analysis Study. *J. Am. Soc. Chem.* **2009**, *131*, 10525−10536.
(34) Li, L.; Meng, F.; Jin, S. High-Capacity Lithium-Ion Battery Conversion Cathodes Based on Iron Fluoride Nanowires and Insights into the Conversion Mechanism. *Nano Lett.* **2012**, *12*, 6030−6037.